# Imaging

# Transmission Computed Tomography Data Acquisition with a SPECT System

Kim L. Greer, C. Craig Harris, Ronald J. Jaszczak, R. Edward Coleman, Laurence W. Hedlund, Carey E. Floyd, and Stephen H. Manglos

*Duke University Medical Center, Durham, North Carolina*

*Phantom and animal transmission computed tomography (TCT) scans were performed with a camera-based single photon emission computed tomography (SPECT) system to determine system linearity as a function of object density, which is important in the accurate determination of attenuation coefficients for SPECT attenuation compensation. Results from phantoms showed promise in providing a linear relationship (R = 0.997) in measuring density while maintaining good image resolution (FWHM = 10.5 mm). Animal images were essentially free of artifacts. Transmission computed tomography scans derived from a SPECT system appear to have the potential to provide data suitable for incorporation in an attenuation compensation algorithm at relatively low (calculated) radiation doses to the subjects.*

Transmission computed tomography (TCT) using single photon (1) and positron (2) emitters can provide additional information regarding the internal nature of the subject under examination. Rhodes et al. (2) have used positron emission tomography with a transmission source to make quantitative measurements of regional extravascular lung densities. Budinger and Gullberg (3) investigated various attenuation compensation methods, including the use of a set of true coefficients determined from a transmission study. They reported that this method allowed for variable attenuation coefficients and was superior to most of the methods; however, it requires two studies.

In this study we have evaluated the ability of a single photon emission computed tomography (SPECT) system to measure the attenuation of technetium-99m ($^{99m}$Tc) in a series of phantoms of known density. Subsequently we measured the resolution of this system and used a dog model for transmission and emission studies. The importance of evaluating SPECT for measuring densities is the possible application of the technique to more accurate attenuation compensation in emission imaging. Such processing is being investigated with positron tomography (4,5). The accuracy of a compensation matrix derived

from a transmission scan would depend primarily on two factors (assuming an adequate photon flux): 1) predictable response to differences in density, and 2) adequate spatial resolution to generate accurate boundaries. We wish to emphasize that this report investigates some characteristics of TCT scanning methodology and does not attempt to validate any specific method of attenuation compensation.

## MATERIALS AND METHODS

### Scanner and Computer Techniques

The SPECT scanner (6) of the Duke University Medical Center, equipped with two gamma cameras*, was used. Only one detector was used in the TCT mode, because the radiation source was mounted directly on one of the cameras. High resolution and ultra-high resolution collimators were used.

Prior to scanning, center of rotation, camera gain adjustments, and flood correction procedures were performed. Flood-correction images contained 30–50 million events. Projection data were acquired at 2° angular increments with 128 linear samples per projection, which corresponds to 3.17 mm/pixel. Data were acquired using continuous gantry motion. Slice thickness was 6.4 mm for most studies. Because we used $^{99m}$Tc as our radiation source, the energy discriminator was set at a centerline of 140 keV and a window width of 18% (full-width at half-maximum [FWHM]). Scans were acquired for 26 min over 360°. A single scan results in up to 32 transverse slices. Data were processed in a mini-computer* and the 128 × 128 reconstructions required about 65 sec of computer time per slice.

Image reconstruction (6) was by filtered backprojection. The filter cutoff frequency corresponded to 1.6 cycles/cm. The filter consists of a ramp function modified by a generalized Hann weighted window (6). The images were normalized such that a value of zero in a region corresponded to air density. The maximum value corresponded to the maximum density in a given image. The absolute value of the maximum pixel is preserved and available so that interslice density comparisons may be made. This required that an object of known density,

## TABLE 1. Analysis of Image Linearity Curve

Slope = 0.0747
Intercept = 0.87
Regression line: $y = 0.075x + 0.87$
Standard error of the estimate = 2.974
Correlation coefficient = 0.997
Standard deviation of intercept = 1.139
Standard deviation of slope = 0.0019



FIG. 2. Transmission computed tomography scan of solid methylmethacrylate sphere mounted within a 22-cm diameter cylinder containing air.
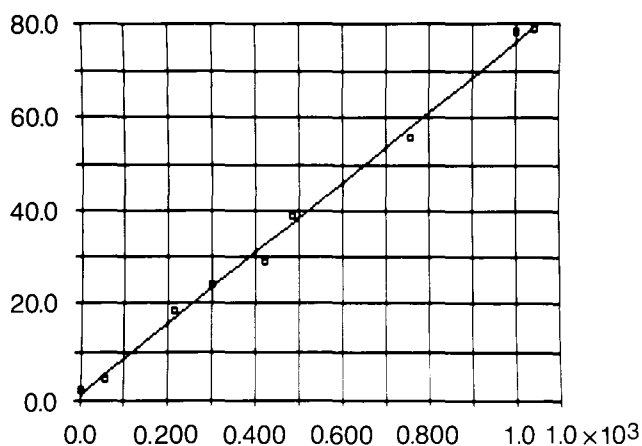
for example a water bottle, be within the scan field of view to calibrate unknown densities to a standard curve.
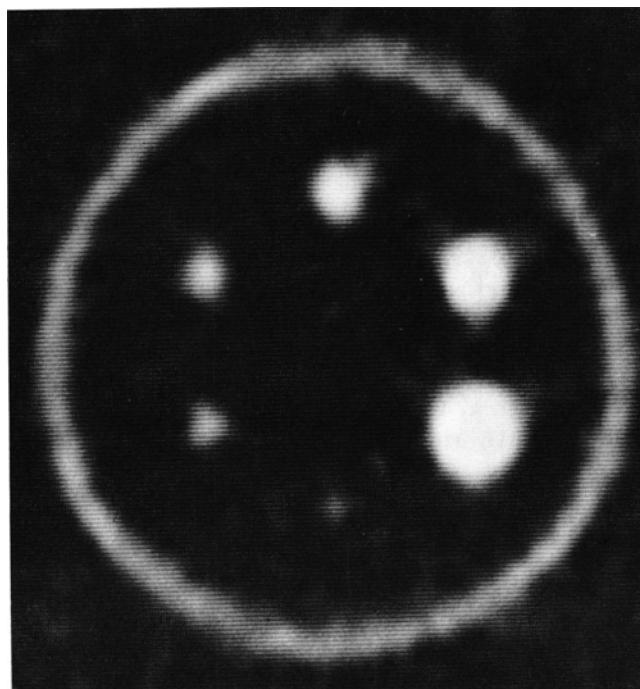
## Radiation Sources

Rectangular radioactive source containers (5 cm × 42 cm × 1.2 cm deep) were constructed. The source length covered the useful field of view of our camera, providing a radiation "sheet" source across the image perpendicular to the axis of rotation. Each source was filled through side access screw holes. The water-filled containers had 70–140 mCi of $^{99m}$Tc added and were mixed to obtain a uniform distribution of radioactivity.

The radioactive source was then mounted so that one of the detectors would intercept any photons passing through and around the sides of the subject. Lead shielding was fitted on the back and sides of the radiation source to reduce stray radiation that might degrade the projection data and to reduce unnecessary exposure to personnel.

We first evaluated the system linearity by imaging objects with a wide range of density. Eight rod-shaped standards of known density (7), 3 cm in diameter, were scanned in air, while supported within styrofoam holders. The long axes of the rods approximately paralleled the axis of rotation (AOR). The densities of the rods ranged from 0 mg/cm$^3$ (air) to 1045 mg/cm$^3$ (slightly greater than water density). A water bottle

of similar diameter was included during the scan of the rods. Rectangular regions of interest were visually located over each individual rod in reconstructed images. The corresponding image values were plotted on linear axes against the actual known density.


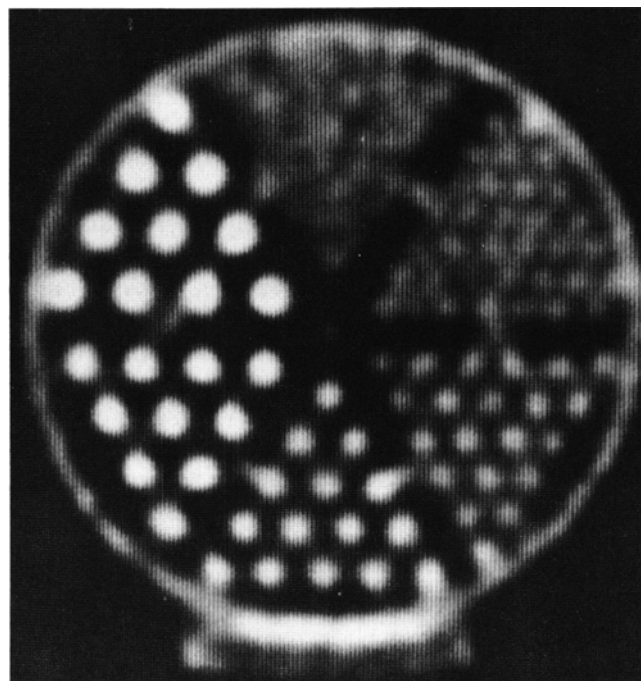
FIG. 1. Plot of system behavior in response to changes in object density. The vertical axis of the graph depicts image region of interest values as a function of density in mg/cm$^3$ (horizontal axis).



FIG. 3. Transmission computed tomography scan of a quality control phantom containing solid rods surrounded by air. Rod diameters are 4.8, 6.4, 7.9, 9.5, 11.1, and 12.7 mm.

**FIG. 4.** Transmission computed tomography scan of calibration rods mounted peripherally about a dog.

Commercially available quality control phantoms* were used to evaluate system resolution. Lucite spheres with diameters of 9.5, 12.7, 15.9, 19.1, 25.4, and 31.8 mm were mounted within an air-filled, 22-cm diameter cylinder and placed in the SPECT unit. The slice thickness was 6.4 mm using the ultra-high resolution collimator and a radius of rotation (ROR) of 13.5 cm. The radiation source typically had a ROR of approximately 5 cm greater than that of the detector. Each slice contained approximately 2.5 million events.

The spheres were replaced with solid lucite rod inserts to further evaluate the system resolution. The rods had diameters

of 4.8, 6.4, 7.9, 9.5, 11.1, and 12.7 mm. The spacing between the rods in any given sector was equal to twice the diameter of the rod. A scan was acquired using the same experimental set-up as the previously described experiment for 26 min per 360° revolution.

A more definitive test to determine system resolution was performed. Steel rods 2.2 mm in diameter were mounted parallel to and away from the AOR with a 15-cm ROR. One rod was located on the AOR and the other was located 10 cm from the AOR. Each slice contained approximately 12 million events in the projection data using the ultra-high resolution collimator. Profiles through the rod were taken from multiple transverse slices and analyzed for FWHM.

## Animal Studies

We scanned animals to ensure that no gross complicating factors such as breathing artifacts would limit the technique to inanimate objects. We chose anesthetized adult dogs for our animal model. Dogs are readily available, easy to work with, and complemented some of our current projects already using SPECT to evaluate the dog thorax with radioactive microspheres and aerosols. The dogs were secured to a polyvinyl-chloride pallet and inserted into the gantry, in supine or prone positions. Scans were performed at the level of the thorax, to include as much of the lungs as possible. Slice thickness was 6.4 mm.

## RESULTS

The transmission scan of the density-calibration rods demonstrated a linear relationship between the density and the pixel values within a given image (Fig. 1 and Table 1).

Figure 2 shows the scan of the six lucite spheres, which vary from 9.5 to 31.8 mm in diameter, mounted in air within the cylinder. Figure 3 shows the resolving ability of the system in a scan of the commercially available phantom. The 6.4 mm diameter rods are readily distinguished from one another. The
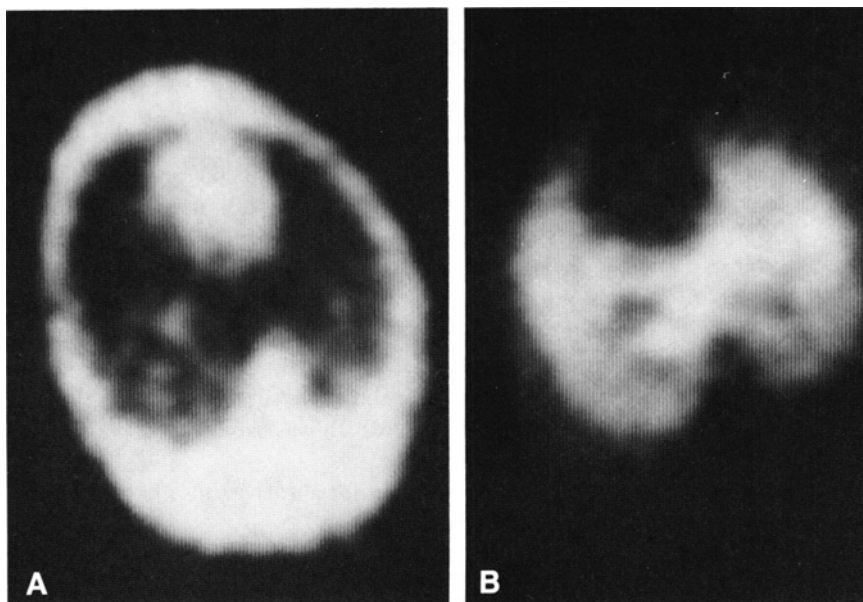


**FIG. 5.** A. Transmission computed tomography scan of a dog. B. SPECT scan of same animal in same position and slice level after administration of $^{99m}$Tc-DTPA aerosols.

resolution in the TCT mode when averaged over several slices was determined to be approximately 10.5 mm FWHM when using the ultra-high resolution collimator.

Figures 4 and 5 present the results of animal studies. Figure 4 shows the eight density calibration rods simultaneously scanned with a dog. Several of the rods are difficult to visualize because of windowing and their very low (essentially air) density. Figure 5A demonstrates chest density as determined using the transmission techniques, and Figure 5B shows ventilation using SPECT and $^{99m}$Tc-DTPA aerosols. The two scans were acquired in succession, the TCT scan first and then during ventilation of the dog. The animal was not moved between scans. The slices represent the same anatomic level. No artifacts were detected in any of the animal or phantom experiments.

## DISCUSSION

The linear density response of the SPECT system (Fig. 1) and the relatively high resolution (Fig. 3) appear to be appropriate for using this technique for derivation of data for attenuation compensation of emission computed tomography images. An advantage to this technique is the ability to determine regional coefficients for use in attenuation compensation, eliminating the use of single, averaged values. Another advantage is the ability to acquire both transmission and emission data on the same machine, allowing for more accurate overlap of emission computed tomography and TCT images. This dual acquisition ability would further facilitate the correlation of emission computed tomography radionuclide distribution with TCT structural landmarks (Fig. 5), and provide better determination of the actual shape of an organ or space. The ability to superimpose the scan images would be the prime benefit of such an approach. Little extra hardware is necessary to mount the radiation source. The patient radiation dose would be significantly lower than with present x-ray TCT systems.

We have calculated (Appendix) that a 70 mCi $^{99m}$Tc source would deliver approximately a 100-mrad dose to the adult torso in a 26-min scan. This single exposure would allow for simultaneously acquiring data from all 11, 22, or 32 slice levels with our current system configuration.

Potential disadvantages include additional radiation dose to the technologist and the additional time required to obtain and process the data. Acquisition and reconstruction times are approximately the same as for a SPECT study. Generation and incorporation of correction matrices for SPECT studies would further increase the total processing time required, but would be expected to provide greater quantitative accuracy.

The benefit of more accurate attenuation compensation may outweigh the burden of increased acquisition and processing time.

## ACKNOWLEDGMENTS

## NOTES

## REFERENCES

1. Maeda H, Itoh H, Ishii Y, et al. Determination of pleural edge by gamma-ray transmission computed tomography. *J Nucl Med* 1981;22:815-817.
2. Rhodes CG, Wollmer P, Fazio F, et al. Quantitative measurement of regional extravascular lung density using positron emission and transmission tomography. *J Comp Assist Tomogr* 1981;5:783-791.
3. Budinger TF, Gullberg GT. Transverse section reconstruction of gamma-ray emitting radionuclides in patients. In: Ter-Pogossian MM, Phelps ME, Brownell GL, eds. Reconstruction tomography in diagnostic radiology and nuclear medicine. Baltimore: University Park Press, 1977:315-342.
4. Huang SC, Hoffman EJ, Phelps ME, et al. Quantitation in positron emission computed tomography: 2. Effects of inaccurate attenuation correction. *J Comp Assis Tomogr* 1979;3:804-814.
5. Huang SC, Carson RE, Phelps ME, et al. A boundary method for attenuation correction in positron computed tomography. *J Nucl Med* 1981; 22:627-637.
6. Greer KL, Jaszczak RJ, Coleman RE. An overview of a camera-based SPECT system. *Med Phys* 1982;9:455-463.
7. Bowyer K, Hedlund L, Vock P, et al. Computer analysis of CT scan images for tissue densitometry. *Appl Opt Instr Med* 1983;347:174-183.
8. MIRD Pamphlet 5: Estimates of specific absorbed fractions for photon sources uniformly distributed in various organs of a heterogeneous phantom. New York: The Society of Nuclear Medicine, 1969.
9. MIRD Pamphlet 10: Radionuclide decay schemes and nuclear parameters for use in radiation-dose estimation. New York: The Society of Nuclear Medicine, 1975.

## APPENDIX

### Absorbed Dose Estimation for Transmission Computed Tomography Procedure Using a $^{99m}$Tc-Source

The following assumptions were used in arriving at an estimate of absorbed dose in an adult human during a chest TCT procedure:

1. Source 5 cm × 42 cm × 2.5 cm deep, placed transverse to axis of rotation.
2. Exposure 0.5 hr, no decay of source ($\bar{A}$ = 500 μCi-hr/mCi).
3. Source centered on torso, 20 cm radius of rotation.
4. Subject: MIRD Adult Phantom Chest (8), 20 cm × 40 cm elliptical, 70 cm long, mass (m) = 17,593 g (density = 1.0).
5. No self absorption in source.
6. $\triangle$ (equilibrium dose constant) = 0.263 g-rad/μCi-hr (9).

As A, m, and $\triangle$ are given above, it is necessary only to estimate $\phi$, the absorbed fraction. A sketch (not shown) of the geometry of the detector–subject relationship indicates that ray-paths through the subject averaged between two and three mean free paths ($2/\mu$-$3/\mu$, $\mu$ = 0.12 cm$^{-1}$, modified for Compton scattering). The absorbed fraction then was taken as 0.9 times the averaged fractional solid angle subtended by the subject as seen from the source, which was estimated as 0.25 (25% interception geometry).

A sample estimate, then, for absorbed dose from a 1 mCi source would be as follows:

$D = (\bar{A}/m)\ \phi\ \triangle = (500/17,593) \times 0.9 \times 0.25 \times 0.26$
$D = 1.68$ mrad